M. Castro, R. Gago, L. Vázquez, J. Muñoz-García, and R. Cuerno, "Energy dependence of the ripple wavelength for ion-beam sputtering of silicon: Experiments and theory". In *AIP Conference Proceedings* 1525 (2013) 380, pp. 380-385. Avalilable in http://dx.doi.org/10.1063/1.4802355

Energy Dependence Of The Ripple Wavelength For Ion-Beam Sputtering Of Silicon: Experiments And Theory

M. Castro[a], R. Gago[b], L. Vázquez[b], J. Muñoz-García[c], and R. Cuerno[c]

[a] *Grupo Interdisciplinar de Sistemas Complejos (GISC) and Grupo de Dinámica No Lineal (DNL), Escuela Técnica Superior de Ingeniería (ICAI),Universidad Pontificia Comillas, E-28015 Madrid, Spain*
[b] *Instituto de Ciencia de Materiales de Madrid, Consejo Superior de Investigaciones Científicas, E-28049 Madrid, Spain*
[c] *Departamento de Matemáticas and GISC, Universidad Carlos III de Madrid, Avenida de la Universidad 30, E-28911 Leganés, Spain*

Abstract. In spite of the efforts devoted for the last 20 years to elucidating ion-beam sputtering (IBS) as an instance of surface self-organization, the classic view on the main mechanism inducing the morphological instability has been recently challenged. We report on the verification of a recent theoretical description of this nanopattern formation process for semiconducting targets, as driven by stress-induced, viscous flow of a thin amorphous layer that develops at the surface [M. Cuerno and R. Cuerno, *Appl. Surf. Sci.* **258**, 4171 (2012)]. Through experiments on silicon as a representative case, we study the dependence of the ripple wavelength with the average ion energy, finding a linear dependence in the 0.3-1 keV range. This is explained within the viscous flow framework, taking into account the energy dependence of the number of displaced atoms generated by collision cascades in the amorphous layer, as predicted by previous models of ion-generated stress. For our analysis, we provide a systematic criterion to guarantee actual linear dynamics behavior, not affected by the onset of nonlinear effects that may influence the value of the ripple wavelength.

Keywords: Nanoscale pattern formation, ion-beam sputtering, ripples, viscous flow, surfaces, morphological instabilities, hydrodynamic models.
PACS: 79.20.Rf, 68.35.Ct, 81.16.Rf, 05.45.-a

INTRODUCTION

Materials surface nanostructuring by ion-beam sputtering (IBS) has received an increased attention in recent years [1,2], due to the potential of this bottom-up procedure for applications in Nanotechnology, and to the interesting issues it arises in Nanoscale Pattern Formation [3] at large. In these experiments, the whole target surface is irradiated by a broad or collimated beam of energetic ions (energies being in the 200 eV to 20 keV range) that impinge onto the former under a well-defined angle of incidence. The capabilities of this technique for efficient nanopatterning have been recognized only recently. Thus, depending on the geometry of the experimental setup and the composition of the targets, it induces ordered ripple (at oblique ion incidence) or dot (at normal ion incidence, or for rotating targets) patterns over large areas (up to 1 cm^2) on metal, semiconductor, and insulator surfaces after a few minutes of irradiation. Both IBS patterns, ripples and dots, share many features, which suggests description within a common framework.

Interestingly, the main features of this process seem to be largely independent of the type of ions and targets employed, provided the latter become amorphous under irradiation [4]; the case of metals falls outside this class, and will not be addressed here, see [1,5]. Under this condition, many experiments [1,2] have given support to the classic view on the mechanism for the ensuing morphological instability. Thus [6], assuming the erosion velocity is proportional to energy deposition due to collision cascades, surface troughs erode faster than peaks, and topographic differences become amplified. Allowing, with Bradley and Harper (BH) [7], for surface diffusion as a counterbalance, a typical wavelength is selected fixing the pattern length scale. This model has provided a paradigm for our understanding of IBS for more than 20 years. Indeed, both [7] and its further developments (for an overview, see [8]) have successfully described various non-trivial features, like instability saturation, pattern coarsening and short range ordering, dependence of pattern properties with experimental parameters for appropriate parameter ranges, etc.

Application of Accelerators in Research and Industry
AIP Conf. Proc. 1525, 380-385 (2013); doi: 10.1063/1.4802355

MORPHOLOGICAL INSTABILITY UNDER IBS

A key prediction common to all BH-type approaches is the formation of a pattern for any ion incidence angle. Hence, the systematic observation for Si targets by Ozaydin et al. [9] on the lack of pattern formation at normal incidence came as a surprise. These authors noted that, under these conditions and for 1 keV Ar^+ ions, patterns were obtained only when intentional seeding with Mo was performed. Actually, similar observations had been reported earlier [10], although at the time no connection to the possible role of (the lack of) impurities had been made. Working also with Si targets at a higher energy (10-40 keV), Carter and Vishnyakov (CV) [10] attributed, rather, their pattern-less surfaces to a process by which, due to momentum transfer, the ion beam would induce down-hill currents on the surface that would tend to smooth out surface features for small incidence angles. Due to the difficulty in the parametrization of this effect, that had been invoked for a particular experiment, its observation remained relatively unconnected from further developments in the modeling of IBS nanopatterns. Further credit for the idea came from studies of ultrasmooth growth of tetrahedral amorphous carbon (ta-C) films by direct ion-beam deposition [11]. Although the average ion energy considered in these Molecular Dynamics (MD) simulations is at the lower limit of the region we are considering, suggestive numerical evidence was indeed provided on the net downhill displacement of the target atoms as induced by the ion beam. This property was then employed to argue in favor of the remarkable smoothing dynamics experimentally seen.

In view of the relatively confusing situation[1] in which different (sometimes conflicting) observations were reported under similar conditions, a number of experiments have been recently addressed at clarifying the situation, focusing on Si targets as a representative case, and taking explicit care on the absence of metallic impurities, see e.g. [13] and references therein. Using as control parameters ion incidence angle to the normal to the unbombarded target, θ, and average ion energy, E, the main conclusions that agree with results by a number of different groups (see e.g. [14]) are [13]: (i) no pattern forms for angles below $\theta = \theta^{exp}_c = 48^o$ (with an experimental uncertainty of 2^o), this angle value being energy independent; (ii) for θ larger than but close to θ_c, the morphological transition at θ^{exp}_c is characterized by a wavelength that diverges as $\lambda = (\theta - \theta_c)^{-1/2}$. These experimental results pose difficulties to previous models of IBS nanopatterning. As mentioned above, the lack of pattern formation for low to intermediate incidence angles is not compatible with BH-type expansions, and cannot be accounted for even by refinement of these, unless additional relaxation mechanisms are invoked, which in principle can be done, see [15-17]. The morphological transition at the energy independent $\theta^{exp}_c = 48^o$ line is of type II in the Pattern Formation terminology [18], nonetheless also associated with BH-type approaches. Such transitions are akin to second order or continuous phase transitions in equilibrium Statistical Physics, in which the characteristic length scale in the system diverges at the transition line (equivalently, the associated wave-vector vanishes continuously). In principle, it has been possible to account for the observed behavior by employing MD data into a continuum framework in which relaxation by viscous flow is introduced *ad-hoc*, see [19] and references therein. One of the conclusions of this work is that the numerical contribution of purely erosive BH-type mechanisms to the surface dynamics is small as compared with effects due to material redistribution; see also [20,21]. A consistent continuum description that can account for all these features within a unified framework has been recently provided by a hydrodynamic model in which the evolution of the surface is controlled by Newtonian viscous flow [22]. Viscoelastic effects can also be taken into account [23], although eventually they do not lead to significant differences in the observed pattern properties for the present ion energy range.

[1] For a view on the status of our understanding of IBS nanopatterns by 2009, see [12] and the papers in the same special issue.

ION-INDUCED SOLID FLOW

In face of the recent experimental data, we have [22] reconsidered the basic ingredients that are required in the continuum description of IBS surface nanopatterns in order to account within a single framework for, at least, the most salient features of the recent experimental picture of the process. Given the large predictive power that ensues when considering the dynamics of material transport at the amorphous layer induced by the ion beam [16,17,24], a natural choice is to focus on this process and leave surface dynamics to arise, rather, as a byproduct of the physical phenomena taking place in the target. Hence, we focus on the dynamics of the amorphous layer that rapidly builds up and stabilizes in mechanical properties (density, thickness) [4,25,26]. However, we resort to a hydrodynamical description that applies to a layer of arbitrary thickness through the study of the appropriate Navier-Stokes equations. In principle, this description should retrieve results for thin layers so that connection with other models [16,17] is feasible in

appropriate parameter ranges [22]. Previous experimental [27] and theoretical [28,29] approaches to the IBS problem through the effects of viscous flow are available, although no general description of the process had been achieved so far.

Note that any fully hydrodynamical approach to these systems has to rely on the fact that the present type of material flow is highly viscous (viscosity of the amorphized layer is in the 10^8 Pa s range [30]), so that actually Stokes flow applies. For simplicity, we take the flowing layer to be Newtonian and incompressible, and of a stationary thickness d, which is achieved by setting the erosion rate at the free interface to equal the amorphization rate at the amorphous/crystalline (a/c) interface. The effect of the ion beam is incorporated as a body force acting in the bulk of the fluid, taking into account the reduction of the ion flux due to non-zero values of the local slope of the free surface. Alternative formulations exist [22,23] in which ion-induced stress is implemented, rather, through an external stress contribution at the free surface. In the thin layer limit, both implementations of stress lead to the exact same physical properties, so that they are indistinguishable. The body force can be written as an amplitude of the force, f_E, times an angular dependence, $\Psi(\theta)$. Hence, this mechanism is reminiscent of the one proposed by CV [10], but crucially not restricted to act along the surface but being present, rather, in the full volume of the flowing layer. The coefficient f_E mediating this mechanism has units of a stress gradient, and its value can be induced [22] from experiments [12] and MD simulations [26], an order of magnitude estimate that agrees with morphological data being 0.42 kg nm^{-2} s^{-2}. Finally, as for the boundary conditions in our flow model, we assume no externally imposed stress, while surface tension σ is taken to act at the free interface, with a no-slip condition being set at the a/c interface.

As mentioned above, this fluid dynamics has an effect on the shape of the free boundary. In order to assess this, one typically considers an initially flat interface and evaluates its stability with respect to a periodic modulation of wave-vector q. For a thin flowing layer such that $dq<<1$, one finds that height perturbations evolve with an amplitude proportional to $\exp(\omega_q t)$, where [22,31]

$$\omega_q = -\frac{f_E d^3 \phi(\theta)}{3\mu} q^2 - \frac{\sigma d^3}{3\mu} q^4. \qquad (1)$$

Here, $\phi(\theta)$ is a derivative of $\Psi(\theta)$ [31], μ is the ion-induced viscosity, and contributions due to purely erosive (BH-type) mechanisms have been neglected. Eq. (1) shows that, in this hydrodynamic formulation, ion-driving and material relaxation couple in a natural, albeit non-trivial, way that generalizes known results. For instance, in the absence of the beam (f_E =0), Eq. (1) reduces to the classic result by Orchard [32] on the rate of smoothing for the free surface of a thin fluid layer, that was employed by Umbach et al. [33] in order to account for the pattern wavelength behavior for experiments on silica targets. For the simplest choice $\Psi(\theta)= \cos\theta$, further detailed analysis of Eq. (1) [22,31] leads to the prediction of a type II morphological transition at an energy independent angle $\theta^{\text{theo}}_{\text{c}}$ =45$^{\text{o}}$, with the same features as in the experiment in the sense that flat surfaces occur for $\theta<\theta^{\text{theo}}_{\text{c}}$ =45$^{\text{o}}$ while ripple formation takes place for larger angles. Moreover, close to the transition the ripple wavelength under pattern forming conditions behaves as $\lambda = 2\pi\,[\sigma/(f_E \sin\theta)]^{1/2}$, where $\lambda=2\pi/q_{\text{c}}$ and q_{c} is the wave-vector value for which Eq. (1) takes its (positive) maximum value. This result agrees quite closely with experiments. In Fig.1 we show a comparison between the latter formula and experimental data obtained [31] for Ar^+ bombardment of Si(100) targets at E=700 eV and a current density of 50 μA cm^{-2}, using a commercial 3 cm beam-diameter Kaufman-type ion gun (VEECO). Metallic contamination is explicitly avoided by employing a sacrificial Si wafer to cover the sample holder, and has been monitored by x-ray photoemission spectroscopy, see details in [31]. Apart from observing $\theta^{\text{exp}}_{\text{c}}$=45$^{\text{o}}$ wih 2$^{\text{o}}$ uncertainty, we see that the experimental $\lambda(\theta)$ dependence follows quite closely the theoretical expectation derived from Eq. (1). All morphological data have been obtained *ex-situ* with a Nanoscope IIIa equipment (Bruker) operating in intermittent contact mode and using silicon cantilevers (Bruker) with a nominal radius of curvature of 8 nm.

Up to this point, the kinetics of the pattern formation process is correctly captured within the viscous flow framework. However, we have not detailed the process that is causing flow to occur in the first place, which would constitute the underlying physical mechanism ultimately inducing the pattern formation. In principle, we attribute it to the stress that sets throughout the amorphous layer as a consequence of the ion-induced damage through the collision cascades occurring in this range of energies. Viscous flow is then the response of the system, trying to relax the external driving thus exerted by irradiation. We aim to inquire further into further implications of such an assumption, in order to assess it on a solid basis.

A simple model of damage-induced stress that is based on linear collision cascades exists [34], in which the generated stress follows, through Hooke's law, from the volumetric strain produced by atom displacements from their equilibrium positions. This stress depends on ion energy, following a square-root law that is modified if one takes into account the

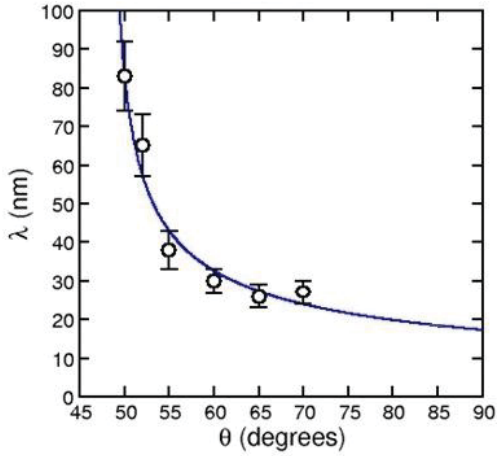

FIGURE 1. Ripple wavelength dependence on the angle of incidence for E = 700 eV, for experiments (circles) performed in the linear regime as estimated by the intrinsic time scale τ, Eq. (2). The solid line is a fit to the behavior predicted by Eq. (1).

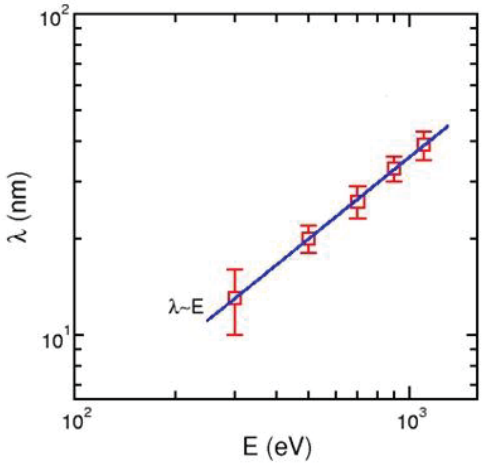

FIGURE 2. Ripple wavelength dependence on the ion energy for experiments at intrinsic times τ, Eq. (2) (squares). The solid line is a fit to a linear dependence.

partial stress relaxation occurring in a time scale comparable to the one needed for collision cascades to relax, in turn orders of magnitude faster than those associated with viscous flow. Davis [35] assumed spike formation to allow displaced atoms to move to the free surface and decrease the effective stress generation. Although spike formation has been shown to account for e.g. Ar^+ experiments on amorphous carbon for energies down to the 50 eV-1 keV range [36], it is believed that processes at these energies are described better by a binary-collision picture [4]. Still, as shown in [37], detailed binary-collision simulations lead to an energy dependence of the generated stress that cannot be distinguished from that in [35] for energies below 2 keV. We employ the latter for analytical convenience leading, for the energy range in our experiments, to [31] $f_E = E^{-7/6-2m}$, where we assume that the thickness of the amorphous layer also scales with energy, as $d = E^{2m}$, typical values of m being between 1/3 and 1/2 as determined from TRIM [38]. Taking into account the spread in the latter exponent value, our assumption on stress as the driving force for the evolution of the target surface leads, through Eq. (1), to an essentially linear dependence of the ripple wavelength with energy as $\lambda = E^{0.92} - E^{1.08}$ [31]. As seen in Fig. 2, such a law is indeed found in our experiments in the 300-1100 eV range. Note, a (close to) linear relation for $\lambda(E)$ contradicts predictions based on the BH mechanism [1,2]. For Ar^+ irradiation in this energy range, it has been also reported for e.g. SiO_2 [33] ---for which surface-confined viscous flow has been advocated---, graphite [39], and amorphous carbon [40]. For Si, previous assessments of the $\lambda(E)$ relation are possibly affected by contamination issues.

The measurements of λ that we have presented assume implicitly that the experiments performed are within the linear regime of evolution for the surface, before nonlinear effects set in that can influence the pattern dynamics and its dependence with system parameters. In fact, experiments do indicate that the very same duration of the linear regime depends on system conditions: Thus, for a fixed ion flux and energy, the onset of nonlinearities takes place earlier at larger incidence angles θ, sinusoidal ripples giving place earlier to more complex morphologies, like faceted and relatively disordered structures [31]. An example is provided in Fig. 3, in which the experimental surface roughness W is plotted as a function of the incidence angle. We can see how, for a fixed fluence (square symbols), W takes a value that is a rapidly increasing function of θ, at least for angles not too close to grazing incidence. This is an indication that, for a given irradiation time, the pattern evolves more rapidly at the higher θ conditions. Analogous observations have been reported by other groups [41]. Interestingly, the viscous flow description provides us with predictions on the characteristics of the linear regime that can be used to perform a self-consistent study of the latter. Thus, given the ensuing exponential rate of growth of height perturbations, one can define a typical time-scale associated with the growth rate of the fastest unstable Fourier mode of the surface, i.e., the one associated with the ripple structure [31],

$$\tau = \frac{E^{7/3-2m}}{J\phi^2(\theta)}, \qquad (2)$$

where J is the average ion flux. Note, τ is the shortest time scale associated with linear evolution, thus it is a safe estimate on the duration of the linear regime for any pair of experimental values (θ, E). Hence, given

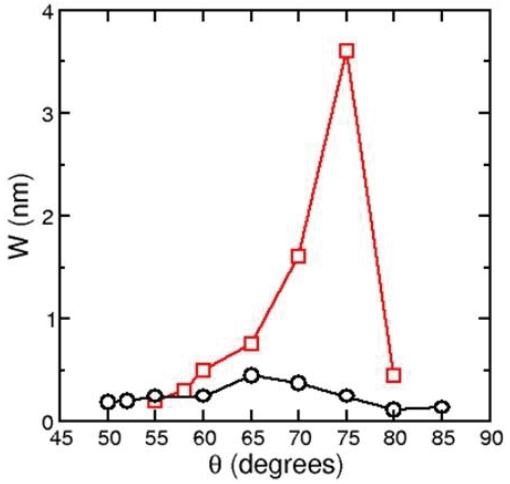

FIGURE 3. Roughness dependence on incidence angle for experiments at E = 700 eV, at constant fluence (squares) and at the time scale τ, Eq. (2) (circles).

we know its value for a reference experimental condition (θ_{ref}, E_{ref}), we can extrapolate it for a different choice by rescaling through Eq. (2). We can thus guarantee that experiments for, say, different values of θ and/or ion E, are within the same linear regime, provided they are performed for the corresponding value of irradiation time prescribed by τ, which we define as an intrinsic timescale. In our case [31], we choose $\theta_{ref} \equiv 55^o$ and $E_{ref} \equiv 700$ eV. In Table I we summarize the intrinsic times for different angles for E = 700 eV. An example of this use is again provided in Fig. 3. Circles correspond to measurements of the roughness at times that relate to one another through Eq. (2). Indeed, now all values of W are quite similar, an indication that the system is at a comparable stage of development of the linear regime for the corresponding experimental conditions. Data shown in figures 1 and 2 have been obtained following a similar procedure.

CONCLUSIONS AND OUTLOOK

We have presented an experimental and theoretical study that elaborates the solid flow description of IBS in silicon, as the case of choice in the recent literature for the class of targets that are amorphous or become so under ion-bombardment at low energies. We have assumed that the main physical mechanism driving the surface dynamics is irradiation-induced damage (stress), implemented as the interplay between atom-displacement and partial relaxation through defect migration. Through the viscous flow form taken by the relaxation of this driving, such an assumption has testable consequences on the morphological dynamics,

TABLE 1. Values of the intrinsic time scale, Eq. (2) (rounded to an integer number of minutes), for fixed ion energy and flux, and different values of the angle of incidence. As reference values, we have used $\theta_{ref} \equiv 55^o$ and $E_{ref} \equiv 700$ eV.

Incidence angle (degrees)	Intrinsic time scale (minutes)
50	69
55	20
60	11
65	8
70	7
75	7
80	9
85	16

via the energy dependence of the ripple wavelength. This provides a natural link between an external forcing exerted through events that occur at the picosecond time scale, and non-trivial surface dynamics unfolding in macroscopic time scales, within a single continuum framework. Specifically, we obtain an (almost) linear relationship $\lambda(E)$ that cannot be reproduced by the BH paradigm, which predicts a decreasing behavior of λ with E. This is actually consistent with similar observations for a number of amorphous or amorphizable targets [33,39,40], for which it seems to be the norm rather than the exception, as was widely believed until recently [1,2]. Another benefit of our results is the systematic exploration of the linear regime for different experimental conditions for which it has a different duration, thanks to the identification of the proper parameter dependence of the relevant time scale.

Overall, these results imply a substantial change with respect to our understanding on the nature of the morphological instability in IBS nanopatterning of monoelemental semiconducting targets. Rather than being purely "erosive" as in BH's picture, the instability sets in as a result of the different exposure to the ion beam of the different regions in the amorphous layer, arising from non-planarity of its free surface. As ultimately dictated by the defect-induced solid flow described above, these local differences imply a larger driving for regions that are more directly exposed to the beam, while dynamics are relatively hampered in regions that receive a reduced flux. For incidence angles above the threshold value, incompressibility makes the fluid "bulge" out, leading to pattern formation. An analogy with fluid flow down an inclined plane for a non-homogeneous gravity field [22] provides an intuitive physical picture.

As a general conclusion, the focus of further efforts should probably remain with the dynamics of the amorphous layer. Naturally, additional features need to be understood, such as the anisotropy of the IBS setup

and its relevance for transitions among different patterns. Also, as suggested by the present work, full understanding of the stress field beneath the surface seems an important avenue for further significant experimental and theoretical improvements. Once the role of impurities, preferential sputtering, and target composition are completely elucidated [42-45], in particular with respect to the mechanism for instability discussed in the present work, a complete picture of IBS nanopatterning can be envisaged to arise that enables full harnessing of this fascinating bottom-up route to self-organized surface nanostructuring.

ACKNOWLEDGMENTS

Partial support has been provided by the Spanish MICINN Grants, Nos. FIS2009-12964-C05-01, -03, and -04, and MEC Grants, Nos. FIS2012-38866-C05-01 and -05, and FIS2012-32349.

REFERENCES

1. W. L. Chan and E. Chason, *J. Appl. Phys.* **101**, 121301 (2007).
2. J. Muñoz-García *et al.*, in *Towards Functional Nanomaterials*, edited by Z. M. Wang, New York: Springer, 2009, pp. 323-398.
3. R. Cuerno *et al.*, *Eur. Phys. J. Special Topics* **146**, 427 (2007).
4. H. Gnaser, *Low Energy Ion Irradiation of Solid Surfaces*, New York: Springer, 1998.
5. F. Buatier de Mongeot, C. Boragno, and U. Valbusa, *J. Phys: Condens. Matter* **21**, 224022 (2009).
6. P. Sigmund, *Phys. Rev.* **184**, 383 (1969); *J. Mat. Sci.* **8**, 1545 (1973).
7. R. M. Bradley and J. M. E. Harper, *J. Vac. Sci. Technol. A* **6**, 2390 (1988).
8. R. Cuerno *et al.*, *Nucl. Instr. Meth. Phys. Res. B* **269**, 894 (2011).
9. G. Ozaydin *et al.*, *Appl. Phys. Lett.* **87**, 163104 (2005).
10. G. Carter and V. Vishnyakov, *Phys. Rev. B* **54**, 17647 (1996).
11. M. Moseler *et al.*, *Science* **309**, 1545 (2005).
12. R. Cuerno *et al.*, *J. Phys.: Condens. Matter* **21**, 220301 (2009).
13. C. S. Madi *et al.*, *Phys. Rev. Lett.* **101**, 246102 (2008); C. S. Madi and M. J. Aziz, *Appl. Surf. Sci.* **258**, 4112 (2012).
14. A. Keller *et al., Nanotechnology* **19**, 135303 (2008).
15. T. Aste and U. Valbusa, *Physica A* **332**, 548 (2004); *New J. Phys.* **7**, 122 (2005).
16. M. Castro *et al.*, *Phys. Rev. Lett.* **94**, 016102 (2005); J. Muñoz-García *et al.*, *J. Phys.: Condens. Matter* **21**, 224020 (2009).
17. J. Muñoz-García, M. Castro, and R. Cuerno, *Phys. Rev. Lett.* **96**, 086101 (2006); J. Muñoz-García, R. Cuerno, and M. Castro, *Phys. Rev. B* **78**, 205408 (2008).
18. M. Cross and H. Greenside, *Pattern Formation and Dynamics in Nonequilibrium Systems*, Cambridge, England: Cambridge University Press, 2009.
19. S. A. Norris *et al., Nature Comm.* **2**, 276 (2011).
20. C. S. Madi *et al.*, *Phys. Rev. Lett.* **106**, 066101 (2011).
21. M. Z. Hossain *et al.*, *Appl. Phys. Lett.* **99**, 151913 (2011).
22. M. Castro and R. Cuerno, *arXiv:1007.2144v1* (2010); *Appl. Surf. Sci.* **258**, 4171 (2012).
23. S. A. Norris, *Phys. Rev. B* **85**, 155325 (2012); *ibid.* **86**, 235405 (2012).
24. J. Muñoz-García *et al.*, *Phys. Rev. Lett.* **104**, 026101 (2010); J. Muñoz-García *et al.*, *J. Phys.: Condens. Matter* **24**, 375302 (2012).
25. M. C. Moore *et al.*, *Nucl. Instr. Meth. Phys. Res. B* **225**, 241 (2004).
26. N. Kalyanasundaram *et al.*, *Mech. Res. Comm.* **35**, 50 (2008).
27. E. Chason *et al.*, *Phys. Rev. Lett.* **72**, 3040 (1994); T. M. Mayer, E. Chason, and A. J. Howard, *J. Appl. Phys.* **76**, 1633 (1994).
28. P. F. A. Alkemade, *Phys. Rev. Lett.* **96**, 107602 (2006).
29. A. S. Rudy and V. K. Smirnov, *Nucl. Instr. Meth. Phys. Res. B* **159**, 52 (1999).
30. S. G. Mayr *et al., Phys. Rev. Lett.* **90**, 055505 (2003).
31. M. Castro *et al., Phys. Rev. B* **86**, 214107 (2012).
32. S. E. Orchard, *Appl. Sci. Res.* **11 A**, 451 (1962).
33. C. C. Umbach, R. L. Headrick, and K. Chang, *Phys. Rev. Lett.* **87**, 246104 (2001).
34. H. Windischmann, *J. Appl. Phys.* **62**, 1800 (1987).
35. C. A. Davis, *Thin Solid Films* **226**, 30 (1993).
36. H. Hofsäss *et al.*, *Appl. Phys. A: Mater. Sci. Proc.* **66**, 153 (1998).
37. B. Abendroth *et al., Appl. Phys. Lett.* **90**, 181910 (2007).
38. B. Ziberi *et al., Phys. Rev. B* **72**, 235310 (2005).
39. S. Habenicht, *Phys. Rev. B* **63**, 125419 (2001).
40. O. Bobes, K. Zhang, and H. Hofsäss, *Phys. Rev. B* **86**, 235414 (2012).
41. S. Macko *et al.*, *New J. Phys.* **13**, 073017 (2011).
42. V. B. Shenoy, W. L. Chan, and E. Chason, *Phys. Rev. Lett.* **98**, 256101 (2007).
43. R. M. Bradley and P. D. Shipman, *Phys. Rev. Lett.* **105**, 145501 (2010).
44. S. Le Roy *et al.*, *Phys. Rev. B* **81**, 161401 (2010).
45. R. M. Bradley, *Phys. Rev. B* **83**, 195410 (2011); *ibid.* **85**, 115419 (2012).